Published in final edited form as:
*Mol Pharm*. 2011 August 1; 8(4): 1390–1400. doi:10.1021/mp200219e.

# A Steroid-Conjugated Magnetic Resonance Probe Enhances Contrast in Progesterone Receptor Expressing Organs and Tumors *In Vivo*

**Preeti A. Sukerkar**[1], **Keith W. MacRenaris**[1], **Thomas J. Meade**[1,*], and **Joanna E. Burdette**[2,*]

[1]Department of Chemistry, Department of Molecular Biosciences, Department of Neurobiology and Physiology, and Department of Radiology, Northwestern University, Evanston, Illinois, 60208

[2]Department of Medicinal Chemistry and Pharmacognosy, University of Illinois at Chicago, Chicago, 60612

## Abstract

Progesterone receptor (PR) is a significant biomarker in diseases such as endometriosis and breast, ovarian, and uterine cancers that is associated with disease prognosis and therapeutic efficacy. While receptor status is currently determined by immunohistochemistry assays, the development of noninvasive PR imaging agents could improve molecular characterization, treatment decisions, and disease monitoring. ProGlo, a progesterone-conjugated magnetic resonance imaging (MRI) contrast agent, was evaluated *in vivo* to determine whether it targets and enhances signal intensity in organs and tumors that express high PR levels. A tissue distribution study indicated that ProGlo accumulates in the PR-rich uterus, which was confirmed by *in vivo* imaging studies. *Ex vivo* images of these organs revealed that ProGlo was distributed in the substructures that express high PR levels. In xenograft tumor models, ProGlo was taken up to a greater extent than the non-functionalized Gd-DO3A in tumors, particularly in PR(+) tumors. The ability to accumulate and enhance signal intensity in PR(+) organs and tumors suggest that ProGlo may be a promising MRI probe for PR(+) diseases.

### Keywords

MRI; Progesterone Receptor; Breast Cancer; Molecular Imaging

## Introduction

Steroid receptors regulate cell processes by controlling gene expression and have emerged as important biomarkers for hormone-dependent diseases such as endometriosis and breast, ovarian, uterine, and prostate cancers. Receptor status is frequently determined for these diseases before treatment is started because many pharmaceuticals, such as tamoxifen, are designed to block the steroid receptor activity that causes tumor growth.[1, 2] Furthermore, the loss of steroid receptor expression induces the disease to become more aggressive and drug-resistant.[3-5] Due to the significant role of steroid receptors in tumor and disease progression,

*Corresponding Authors: Thomas J. Meade, PhD Department of Chemistry, Molecular Biosciences, Neurobiology and Physiology, and Radiology Northwestern University 2145 Sheridan Road, Evanston, IL 60208. tmeade@northwestern.edu Joanna E. Burdette, PhD College of Pharmacy Department of Medicinal Chemistry and Pharmacognosy University of Illinois at Chicago 900 South Ashland, Chicago, IL 60612 joannab@uic.edu.

Supporting Information Available
Figures S1, S2, and S3. This information is available free of charge via the Internet at http://pubs.acs.org/.

these proteins represent excellent imaging targets for noninvasive molecular characterization and monitoring of cancers and other hormone-related diseases.[6]

Estrogen receptor (ER) and estrogen-regulated progesterone receptor (PR) status are frequently used to guide treatment and predict prognosis in diseases such as endometriosis and uterine and breast cancers.[4, 7, 8] The presence of both receptors correlates with the survival rate of breast cancer patients,[9] while decreased PR in ER+ tumors is associated with tamoxifen resistance, although the mechanism of resistance is unknown.[10] Overexpression of PR is associated with the probability of breast tumor responsiveness to tamoxifen and higher survival, while aggressive and metastatic ER+/PR(-) tumors are more likely to respond to aromatase inhibitors.[10-12] Since expression of PR in breast tumors may reflect activation of the growth factor pathway Her2/neu, establishing the PR status may determine if a patient will respond to monoclonal antibody treatments directed against the Her2/neu receptor.[13] Endometriosis is staged based on PR expression and is associated with the development of endometrial cancer. Progesterone is often used as a therapeutic agent for shrinking endometriotic lesions and for slowing the growth of endometrial cancers.[8] Therefore, delineating whether or not diseased tissues express PR is crucial to determining the optimal therapeutic agent for the patient and ultimately improves survival.

PR levels are measured by *in vitro* immunohistochemistry assays of biopsy samples, but noninvasive imaging techniques could offer several advantages.[14, 15] Imaging would likely capture the intrinsically heterogeneous PR levels within whole specimen and allow for measurement of PR levels in benign disease, primary tumor, and metastatic lesions. In addition, changes in PR status could be monitored over time.[16] Finally, noninvasively imaging PR levels in animal models of spontaneous and drug-resistant disease might elucidate molecular pathways responsible for progression and tools for novel drug discovery.

Several PR-targeted positron emission tomography (PET) agents based on both steroidal and non-steroidal progestins have been developed.[6, 17, 18] Despite success *in vitro* and in animal models, a steroidal progestin-based PET agent that was tested in humans was rapidly metabolized by 20-hydroxysteroid dehydrogenase, rendering it ineffective.[19] In addition, PET suffers from low resolution, limited anatomical detail, short half-life of the commonly used $^{18}$F tracer, and the requirement of a nearby cyclotron.[20-22] In contrast, magnetic resonance imaging (MRI) offers high spatial resolution, excellent soft tissue contrast, chemically stable contrast agents, and no exposure to radiation.[23-27] MRI is increasingly used in breast cancer imaging and has been proven more effective than mammography, computed tomography, and PET.[20, 28-30] For patients with familial risk of breast cancer, lesions tend to form quickly and have varying appearances using mammography.[31] When a patient has a positive mammography and biopsy, MR imaging is used to identify other lesions, particularly in the contralateral breast.[28] Functional imaging agents for breast lesions that monitor steroid receptor status and possess the high quality spatial resolution of MRI might provide a more effective secondary line diagnosis.

While higher affinity nonsteroidal progestins are being studied for PET, the presence of a bulky Gd(III) chelate on these progestins would likely prevent PR binding. An alternative approach in the development of PR-targeted MR contrast probes used the steroidal RU-486 or 21-hydroxyprogesterone.[32-34] The C21 hydroxyl group on 21-hydroxyprogesterone provides a site for attachment of a Gd(III) chelate while maintaining high affinity for PR.[33] In addition, the steric hindrance due to the chelate will likely decrease metabolism by 20-hydroxysteroid dehydrogenase.[35] Finally, the toxicity and biological profiles of progesterone have been extensively studied as compared to nonsteroidal drugs, making it a suitable starting point for the development of PR-targeted MRI contrast agents. These 21-

hydroxyprogesterone-derived MR agents specifically targeted and bound to PR as demonstrated by activation of PR-regulated transcription *in vitro*.[33] These probes successfully enhanced MR signal in PR(+) over PR(-) breast cancer cells.[33] One of these agents, ProGlo, was selected for further evaluation *in vivo* and in the current study specifically targeted PR-rich organs *in vivo* and preferentially accumulated in PR(+) human breast tumor xenografts.

## Materials and Methods

### General Methods

Unless noted, materials and solvents were purchased from Sigma-Aldrich Chemical Co. (St. Louis, MO) and used without further purification. $GdCl_3 \cdot 6H_2O$ and 1,4,7,10-tetraazacyclododecane (cyclen) were purchased from Strem Chemicals (Newburyport, MA) and used without further purification. Unless noted, all reactions were performed under a nitrogen or argon atmosphere. Acetonitrile was purified using a Glass Contour Solvent system. Deionized water was obtained from a Millipore Q-Guard System equipped with a quantum Ex cartridge (Billerica, MA). Thin-layer chromatography (TLC) was performed on EMD 60F 254 silca gel plates. Visualization of the developed chromatogram was performed by CAM stain and platinum stain. Standard grade 60 Å 230-400 mesh silca gel (Sorbent Technologies) was used for flash column chromatography. $^{1}H$ and $^{13}C$ NMR spectra were obtained on a Bruker 500 MHz Avance III NMR Spectrometer or a Varian Inova 400 MHz NMR spectrometer with deuterated solvent as noted. Electrospray ionization mass spectrometry (ESI-MS) spectra were taken on a Varian 1200 L single-quadrupole mass spectrometer. High resolution mass spectrometry data was aquired on an Agilent 6210 LC-TOF (ESI, APCI, APPI). Analytical reverse-phase HPLC-MS was performed on a Varian Prostar 500 system with a Waters Atlantis C18 column (4.6 × 250, 5 μm). This system is equipped with a Varian 380 LC ELSD system, a Varian 363 fluorescence detector, a Varian 335 UV-vis detector, and a Varian 1200L Quadrupole MS detector. Preparative runs were performed on a Waters Atlantis C18 column (19 × 250, 10 μm). Mobile phase consisted of water (solvent A) and HPLC-grade acetonitrile (solvent B).

### Synthesis

**{1,4,7-tris(carboxymethyl)-10-[10-(6-(2-((10*R*,13*S*,17*S*)-10,13-dimethyl-3-oxo-2,3,6,7,8,9,10,11,12,13,14,15,16,17-tetradecahydro-1*H*-cyclopenta[*a*]phenanthren-17-yl)-2-oxoethoxy)hexyl]-1,4,7,10-tetraazacyclododecanato}gadolinium (ProGlo)—**The synthesis and purification of Proglo were performed as previously published.[33]

**1,4,7-Tris(*tert*-butoxycarbonylmethyl)-1,4,7,10-tetraazacyclododecane (1)—** Cyclen (5 g, 29.0 mmol) and $NaHCO_3$ (5.50 g, 65.5 mmol) were dissolved in anhydrous acetonitrile (150 mL). *tert*-butylbromoacetate (9.60 mL, 65.0 mmol) was added dropwise under nitrogen to the solution. The mixture was stirred at room temperature under nitrogen for 48 hours. After filtration of the $NaHCO_3$ and removal of the acetonitrile by rotary evaporation, the remaining crude product was dissolved in dichloromethane and washed with water. Recrystallization from toluene yielded an off-white solid (6.05 g, 40%). $^{1}H$ NMR (500 MHz, chloroform-d) δ 3.38 – 2.88 (b, 21H), 1.47 (s, 27H). $^{13}C$ NMR (125 MHz, d-chloroform) δ 170.76, 169.87, 82.07, 81.93, 58.49, 51.59, 51.17, 49.41, 47.79, 28.47, 28.43. ESI-MS *m/z* $[M + H]^+$: 515.1

**{1,4,7-Tris(*tert*-butoxycarbonylmethyl)-1,4,7,10-tetraazacyclododecanato}gadolinium (Gd-DO3A)—**A solution of **1** (0.750 g, 1.46 mmol) in trifluoroacetic acid (2 mL) was stirred at room temperature for several hours. After

removal of the acid, the crude free ligand was taken up in water and the pH was adjusted to 6. A solution of $GdCl_3$ in water was added slowly while maintaining the pH between 5.5 and 6.5. The solution was heated to 60 °C and stirred under nitrogen. The pH was monitored and adjusted to between 5.5 and 6.5 as needed until there was no longer a change. The reaction mixture was lyophilized and then purified by preparative HPLC using a ramp from 0 to 100% B over 20 minutes to afford a white solid (0.470 g, 94%). HRMS (ESI) *m/z*: found 502.09519 $[M + H]^+$ (calcd 502.09398 for $C_{14}H_{24}N_4O_6Gd$). See **Supporting Information** for analytical HPLC trace of purified Gd-DO3A.

**1,4,7-Tris(*tert*-butoxycarbonylmethyl)-10-hexyl-1,4,7,10-tetraazacyclododecane (2)—**To a mixture of 1-bromohexane (99.0 μL, 0.705 mmol), **1** (0.500 g, 0.971 mmol), and $K_2CO_3$ (0.290 g, 2.10 mmol) in anhydrous acetonitrile was added 40% tetrabutylammonium hydroxide (30 μL). The mixture was heated at 65 °C for 16 hours. After filtration of the $K_2CO_3$ and removal of the acetonitrile by rotary evaporation, the residue was purified by flash chromatography (with dichloromethane and methanol (15:1) to yield the final product (0.318 g, 55%). $^1$H NMR (400 MHz, chloroform-d) δ 3.42 – 2.33 (m, 21H), 1.70 (m, 4H) 1.48 – 1.26 (m, 29H), 1.01 (t, *J* = 7.4 Hz, 6H), 0.87 (m, 2H). $^{13}$C NMR (100 MHz, d-chloroform) δ 172.76, 94.625, 82.93, 82.62, 59.19, 56.54, 55.92, 54.65, 50.67, 31.97, 28.12, 27.35, 24.41, 22.71, 19.98, 14.15. ESI-MS *m/z* $[M + Na]^+$: 621.7

**{1,4,7-Tris(*tert*-butoxycarbonylmethyl)-10-hexyl-1,4,7,10-tetraazacyclododecane}gadolinium (Gd-Hexyl-DO3A)—**A solution of **2** (0.318 g, 0.531 mmol) in formic acid (1 mL) was stirred at 60 °C overnight. After removal of the formic acid, the crude free ligand was metalated and purified as described above for Gd-DO3A to yield a white solid (0.136 g, 44%). HRMS (ESI) *m/z*: found 586.18851 $[M + H]^+$ (calcd 586.18804 for $C_{20}H_{36}N_4O_6Gd$). See **Supporting Information** for analytical HPLC trace of purified Gd-Hexyl-DO3A.

## Octanol-Water Partition Coefficients

ProGlo, Gd-DO3A, and Gd-Hexyl-DO3A (1 mg) were dissolved in 1 mL of a 1:1 mixture of water:1-octanol. After shaking for 30 seconds, the tube was placed on a rotator for gentle mixing for 4 hours, and was then allowed to equilibrate for 10 hours. Gd(III) concentration in each layer was determined by ICP-MS. Partition coefficients were calculated from the equation $\log P = \log(C_o / C_w)$, where logP is the logarithm of the partition coefficient, $C_o$ is the concentration of Gd in the 1-octanol layer, and $C_w$ is the concentration of Gd in the water layer.[32]

## Relaxation Time Measurements

Solutions of Gd-Hexyl-DO3A and Gd-DO3A were prepared in 500 μL of nanopure water for $T_1$ and $T_2$ acquisition. Due to the hydrophobicity of ProGlo, concentrated stock solutions were made in dimethyl sulfoxide (DMSO) and diluted into water to a final concentration of 1% DMSO before $T_1$ relaxation time measurement. $T_1$ and $T_2$ relaxation times were measured on a Bruker mq60 NMR analyzer equipped with Minispec V2.51 Rev.00/NT software (Billerica, MA, USA) operating at 1.41 T (60 MHz) and 37 °C. $T_1$ relaxation times were measured using an inversion recovery pulse sequence (t1_ir_mb) using the following parameters: 4 scans per point, 10 data points for fitting, monoexponential curve fitting, phase cycling, 10 ms first pulse separation, and a recycle delay and final pulse separation ≥ $5T_1$. $T_2$ relaxation times were measured using a Carr–Purcell–Meiboom–Gill (CPMG, t2_cp_mb) pulse sequence using the following parameters: 4 scans per point, 100–5000 data points for fitting (longer $T_2$ = more data points for fitting to produce a good monoexponential curve fit), monoexponential curve fitting, phase cycling, 1 ms pulse

separation (unless otherwise specified), and a 15 s recycle delay. The Gd(III) concentration of each solution was determined using ICP-MS. The inverse of the relaxation time ($1/T_1$ or $1/T_2$, $s^{-1}$) was plotted against Gd(III) concentration (mM) and fitted to a straight line with $R^2 > 0.99$. The slope of the fitted line was recorded as the relaxivity, $r_1$ or $r_2$.

### General Cell Culture

Dulbecco's modified phosphate buffered saline (DPBS), media, sera, and TrypLE were purchased from Invitrogen (Carlsbad, CA). Cell culture consumables (flasks, plates, etc.) were purchased from VWR (Radnor, PA). Charcoal dextran stripped FBS was purchased from Atlanta Biologicals (Lawrenceville, GA). MDA-MB-231 cells obtained from ATCC (Rockville, MD) were cultured using phenol red-free α-MEM (modified to contain 20 ng/mL insulin) supplemented with 10% FBS (characterized) or with 10% charcoal dextran stripped FBS. T47D cells obtained from ATCC (Rockville, MD) were cultured using phenol red free RPMI 1640 (modified to contain 1.0 mM sodium pyruvate, 1.0 mM HEPES, and 4.5 g/L glucose) supplemented with 10% FBS or 10% charcoal dextran stripped FBS. Prior to all experiments, cells were plated in media containing non-charcoal dextran stripped media. The plating media was replaced with media containing stripped FBS for 24 hours and was then replaced with fresh stripped media for another 24 hours. Experiments and incubations were done in a 5.0% $CO_2$ incubator at 37 °C unless otherwise noted. Cells were harvested by incubation with 0.25% TrypLE for 10 minutes at 37 °C in a 5.0% $CO_2$ incubator.

### Cellular Uptake Studies

Contrast agents were dissolved in DMSO and diluted into the appropriate media (containing stripped FBS) for each cell line (T47D and MDA-MB-231) so that the final amount of DMSO was 0.125% v/v in the media at concentration of 0.125 mM of contrast agent. Cells were incubated with 0.125 mM contrast agent for 1, 4, 10, and 24 hours (all conditions performed in triplicate). After incubation, the media was removed, and the cells were rinsed twice with DPBS. These cells were trypsinized, counted, and analyzed for Gd(III) content by ICP-MS.

### Cell Counting Using Guava EasyCyte Mini Personal Cell Analyzer (PCA) System

After cell harvesting, an aliquot of the cell suspensions were mixed with Guava ViaCount reagent and allowed to stain at room temperature for at least 5.0 minutes (no longer than 20 minutes). Stained samples were vortexed for 10 seconds and counted. Percent cell viability determined via manual analysis using a Guava EasyCyte Mini Personal Cell Analyzer (PCA) and ViaCount software module. For each sample, 1000 events were acquired with dilution factors that were determined based upon optimum machine performance (~ 25 — 70 cells/μL). Instrument reproducibility was assessed daily using GuavaCheck Beads and following the manufacturer's suggested protocol using the Daily Check software module.

### Animal Experiments

Female CD-1 mice and female Balb/C athymic nude mice were acquired from Harlan (Indianapolis, IN) and housed under pathogen free conditions. All animal studies were conducted at University of Illinois at Chicago and Northwestern University in accordance with the National Institutes of Health Guide for the Care and Use of Laboratory Animals and established institutional animal use and care protocols.

### Tissue Distribution

ProGlo, Gd-Hexyl-DO3A, and Gd-DO3A were each dissolved in DMSO such that 0.15 mmol agent per kg body weight was injected into each CD-1 mouse (mice were

approximately 25 g each). Intravenous injections could not be administered due to the insolubility of ProGlo. Thus, the agents (100 μL volume) were injected intraperitoneally, and tissues were harvested at 2, 6, and 24 hours after injection. Fat was removed from the tissue to ensure that the Gd(III) levels in only the tissue of interest was determined. Five mice per time point were used for ProGlo and Gd-DO3A, and three mice per time point were used for Gd-Hexyl-DO3A. Gd(III) content was determined by ICP-MS.

### Tumor Xenograft Models

Due to low circulating estradiol levels in nude mice, a 17β-estradiol pellet (Innovative Research of America, Sarasota, FL, 70-day release, 0.72 mg/pellet) was implanted subcutaneously in the nape of the neck to ensure growth of estrogen-dependent T47D cells. Two to seven days later, T47D and MDA-MB-231 ($1\text{-}2 \times 10^6$) cells in DPBS were suspended in Matrigel (1:1 volume) and injected subcutaneously into the rear flank (T47D cells on the right side and MDA-MB-231 cells on the left). Mice were monitored for tumor growth every two to three days after injection of cells. MR images were acquired two to three weeks after xenografting when tumors were palpable.

### In Vivo MR Imaging

CD-1 mice (n = 3 per compound) were imaged before injection and at 2, 6, and 24 hours after intraperitoneal injection with ProGlo or DO3A (dissolved in 50 μL DMSO), consistent with the tissue distribution study. Xenografted nude mice were injected either intraperitoneally (n = 2 per compound) or subcutaneously (n = 4 for ProGlo and n = 3 for Gd-DO3A). During imaging, mice were maintained under anesthesia (1-3% isoflurane) but were allowed to wake up and recover between imaging time points. Tubing containing heated water was positioned under the mouse to keep a constant body temperature. All MR imaging was performed on a 89 mm bore size PharmaScan 7.05 T MR imager fitted with shielded gradient coils (Bruker BioSpin, Billerica, MA, USA) using a RF RES 300 1H 089/038 quadrature transmit receive volume coil (Bruker BioSpin, Billerica, MA, USA).

For *in vivo* imaging of the uterus and ovaries, $T_2$-weighted RARE (Rapid Acquisition with Rapid Echo) scans without fat suppression were used to detect tissues of interest, particularly the ovary: TR = 3000 ms, TE = 11.739 ms, rare factor = 8, effective TE = 46.956 ms, FOV = 35 × 35 $mm^2$, matrix size = 256 × 256, slice thickness = 1.0 mm, interslice distance = 1.0 mm. Standard $T_1$-weighted multislice multiecho (MSME) scans with fat suppression were used for imaging the uterus, ovaries, and xenografts: TR = 700 ms, TE = 10.635 ms, FOV = 35 × 35 $mm^2$, matrix size = 256 × 256, slice thickness = 1.0 mm, interslice distance = 1.0 mm. Images were analyzed using ImageJ. Contrast-to-noise ratios (CNRs) were calculated using the equation $CNR = (SI_{Tissue} - SI_{Muscle})/\sigma_{noise}$ where $SI_{Tissue}$ is the signal intensity in the tissue of interest (uterus or ovary), $SI_{Muscle}$ is the signal intensity in the muscle, and $\sigma_{noise}$ is the standard deviation of the noise. At least two slices were analyzed per mouse unless the tissue of interest was clearly demarcated in only one slice.

CNRs in the xenograft images were calculated using the equation $CNR = (SI_{Tissue} - SI_{Muscle})/\sigma_{noise}$ where $SI_{Tumor}$ is the signal intensity in the tumor, $SI_{Muscle}$ is the signal intensity in the muscle, and $\sigma_{noise}$ is the standard deviation of the noise. CNRs were analyzed in two to three axial slices per mouse.

### Ex Vivo *MR Imaging*

CD-1 mice were injected with 5 IU pregnant mare serum gonadotropin (PMSG) intraperitoneally in 100 μL saline. After two days, the mice were injected intraperitoneally with ProGlo or Gd-DO3A similarly to the tissue distribution and imaging studies. Two

hours after injection, the mice were euthanized and the uterus and ovaries were removed en bloc from each animal. Each uterus was cut in half such that each piece contained one ovary and half the uterus. The tissues were embedded in low melting temperature agarose and imaged using a 3D FLASH (Fast Low Angle Shot**)** pulse sequence with the following parameters: TR = 20.0 ms, TE = 4.368 ms, flip angle = 15.0°, FOV = 250 × 250 × 100 $mm^3$, matrix size = 256 × 256 × 100. MR imaging was performed on a 89 mm bore size PharmaScan 7.05 T MR imager fitted with shielded gradient coils (Bruker BioSpin, Billerica, MA, USA) using a RF RES 300 1H 089/023 mouse brain transmit receive volume coil.

### ICP-MS Sample Preparation and Instrument Parameters

For octanol-water, relaxivity, and cell studies, ACS reagent grade nitric acid (70%) was added to solutions of the agent in water or 1-octanol, cell suspensions and media (for a 1.0:1.0 v/v sample:nitric acid) in 15-mL conical tubes and placed at 65 °C for at least 4.0 hours to allow for complete sample digestion. For samples in 1-octanol, tubes were vented every 30 minutes due to buildup of pressure. Nanopure $H_2O$ and internal standard (either indium or multi-element) were added to produce a final solution of 3.0% nitric acid (v/v) and 5.0 ng/mL internal standard. Gadolinium standards were prepared at 0.10, 0.25, 0.50, 1.0, 5.0, 10, 25, and 50 ng/mL concentrations with 3.0% nitric acid (v/v) and internal standard final concentrations. Standard concentrations were prepared from commercially available standards (Sigma-Aldrich Chemical Co., St. Louis, MO).

For tissue distribution and xenograft studies, 1.0 mL ACS reagent grade nitric acid (70%) was added to 50 mL conical tubes containing pre-massed tissue samples. The tubes were capped and heated at 75 °C for 4 hours. The tubes were vortexed and vented every 30 minutes during this digestion process. After the tissue was liquefied, the tubes were allowed cool to room temperature. The acid mixtures were then passed through 0.2 μm PTFE filters. A portion of each of these samples was placed in a clean pre-massed 15 mL conical tube followed by addition of nanopure $H_2O$ and indium internal standard to produce a final solution of 3.0% nitric acid (v/v) and 5 ng/mL internal standard up to a total sample volume of 10 mL.

ICP-MS was performed on a computer-controlled Thermo Elemental (Waltham, MA) PQ ExCell Inductively Coupled Plasma Mass Spectrometer equipped with a CETAC 500 autosampler. Each sample was acquired using 1 survey run and 3 main (peak jumping) runs. The isotopes selected were $^{156,157}Gd$, as well as $^{115}In$ and $^{165}Ho$ (as internal standards for data interpolation and machine stability).

## Results

### Synthesis, Relaxivity, and Octanol-Water Partition Coefficients

PR-targeted MR agents were previously synthesized with a wide range in cellular permeability.[33] Due to its high cellular permeability and specific retention in PR(+) breast cancer cells, ProGlo was chosen for comparison to non-targeted contrast agents *in vitro* and *in vivo*. PR-targeted ProGlo and the two non-targeted control agents (Gd-Hexyl-DO3A and Gd-DO3A), are shown in **Figure 1**. Gd-DO3A is the Gd(III) chelate of 1,4,7,10-tetraazacyclododecane-1,4,7-triacetic acid (DO3A) that forms the MR-active moiety of ProGlo. Gd-Hexyl-DO3A, a derivative of Gd-DO3A containing a six-carbon aliphatic tail, was synthesized to control for possible effects of the aliphatic linker on the biological properties of ProGlo.

The synthesis of ProGlo was previously reported.[33] The syntheses of the nontargeted controls are shown in **Scheme 1**. To synthesize Gd-DO3A, *tert*-butylbromoacetate was

coupled to the 1,4, and 7 positions on cyclen to form DO3A-tris-*tert*-butyl ester (**1**). Following removal of the *tert*-butyl protecting groups with trifluoroacetic acid, the free ligand was metalated with $GdCl_3$ in water at pH = 5.5 to 6.5. Purification of the final compound was performed by preparative HPLC. Gd-Hexyl-DO3A was synthesized in a similar manner. Addition of 1-bromohexane to the secondary nitrogen on **1**, followed by removal of the *tert*-butyl protecting groups with formic acid yielded the free ligand (**2**). This compound was then metalated with $GdCl_3$ in water at pH = 5.5 to 6.5. Purification or the final contrast agent was performed by preparative HPLC.

Longitudinal and transverse relaxivities ($r_1$ and $r_2$) conducted at 1.41 T and 37 °C are summarized in **Table 1**. The relaxivity of ProGlo previously reported at 4.7 T and 21 °C is shown for comparison. The relaxivities of all three agents were similar to those reported for clinically used contrast agents, approximately 4 – 5 $mM^{-1}s^{-1}$. However, ProGlo and Gd-Hexyl-DO3A had 30-40% higher $r_1$ and $r_2$ than Gd-DO3A, most likely due to the higher molecular weights and aggregation of these amphiphilic agents.

Octanol-water partition coefficients (logP), summarized in **Table 1**, were measured to determine the hydrophobicity of the agents, which correlates to the cellular permeability and the tissue distribution [36, 37]. The previously reported octanol-water partition coefficient for ProGlo had been measured using the shake flask method and determining the mass of compound in each layer.[33] The current study used the shake flask method followed by ICP-MS to determine Gd(III) concentration in each layer, allowing for improved accuracy with the sacrifice of less material. The positive logP value for ProGlo indicated its hydrophobic nature, and the negative logP values for the non-targeted agents were characteristic of high water-solubility. The literature value for the logP of 21-hydroxyprogesterone is shown for comparison.[38] ProGlo was significantly more hydrophobic than either of the non-targeted controls due to the presence of the lipophilic steroid. In addition, the alkyl chain in Gd-Hexyl-DO3A resulted in increased hydrophobicity relative to Gd-DO3A, indicating that the presence of the carbon linker in ProGlo further contributed to its high partition coefficient.

## ProGlo Accumulates in Human Breast Cancer Cells

To determine the cellular permeability of the agents, cellular uptake of ProGlo and the non-targeted agents was studied in PR(+) T47D and PR(-) MDA-MB-231 human breast cancer cells (**Figure 2**). As expected, the uptake mirrored the octanol-water partition coefficients. The uptake of the hydrophobic ProGlo was highest in both cell types, followed by Gd-Hexyl-DO3A. The hydrophilic nature Gd-DO3A reduced its cellular permeability, resulting in low cellular uptake. Furthermore, the uptake of ProGlo was higher in the PR(+) cells than in the PR(-) cells at the 10 and 24 hour incubation times, indicating that ProGlo preferentially targeted PR in cells and was retained longer inside these cells due to PR binding as previously reported.[33]

## *PR-rich Tissues Accumulate ProGlo* In Vivo

Tissue distribution studies were carried out to determine whether the steroid-modified contrast agent was specifically retained within tissues that express high levels of progesterone receptor *in vivo*. Each agent was dissolved in DMSO and injected intraperitoneally into female CD-1 mice (0.15 mmol/kg body weight). The organs were harvested at 2, 6, and 24 hours after injection. Total Gd(III) per gram of tissue is shown in **Figure 3**. Clearance of the agents mirrored the trend in octanol-water partition coefficients. Hydrophobic ProGlo was likely cleared hepatically, hydrophilic Gd-DO3A was cleared renally, and Gd-Hexyl-DO3A was cleared by both liver and kidney due to its mid-range partition coefficient[39] and its initial high Gd(III) levels in these tissues.

Not surprisingly, high levels of ProGlo were detected in the liver. In addition, ProGlo accumulated in the uterus, ovary, and mammary, which contain high levels of PR.[40] In the uterus, ProGlo was retained and maintained a Gd(III) level significantly higher than in the muscle (which served as a negative control) for up to 24 hours. Importantly, ProGlo did not accumulate in other abdominal tissues or within the fat, which was originally a concern due to the hydrophobicity of the agent (**Supporting Information**).[39] Despite the high levels of Gd-DO3A in most tissues at the 2 hour time point, it was not significantly retained in those tissues by 6 hours post-injection as compared to ProGlo. Gd-Hexyl-DO3A was cleared by the kidney and liver with very low levels detected in other tissues. The levels of Gd-Hexyl-DO3A were significantly lower than ProGlo in the uterus, ovaries, and mammary tissues at all time points, and the levels of Gd-DO3A were significantly lower than ProGlo in these tissues at 6 and 24 hours post-injection. These results indicate that ProGlo, unlike the two control agents, targeted and was retained in PR-rich tissues *in vivo*.

## MRI Contrast-to-Noise Ratio in the Uterus is Enhanced by ProGlo in Vivo

To establish a correlation between the tissue distribution of our agents and the ability to image steroid receptor expression at corresponding time points, CD-1 mice were injected with ProGlo or Gd-DO3A, and their uteri and ovaries were imaged. Gd-Hexyl-DO3A was not imaged because it was present in very low levels in the tissues of interest for all time points in the tissue distribution study. The average contrast-to-noise ratio (CNR) over three mice per agent at each imaging time point is shown in **Figure 4**. After injection of ProGlo, the right and left sides of the uterus had significantly increased CNR relative to the CNR before injection through 24 hours post-injection, correlating with the retention of Gd(III) in the uterus in the tissue distribution study. Injection of Gd-DO3A, however, resulted in no significant changes in CNR in the uterus or ovaries. These results provide definite evidence that ProGlo accumulated in PR-rich tissues, while Gd-DO3A did not.

## ProGlo Localizes to Specific Regions of High PR Expression Within the Uterus and Ovaries

To investigate the differential enhancement of organ substructure in mice injected with ProGlo versus those injected with Gd-DO3A, *ex vivo* imaging of the uterus and ovaries was performed. In order to increase organ size, mice were superovulated by injection of pregnant mare serum gonadotropin (PMSG) two days prior to imaging. PMSG stimulates ovarian production of estrogen, which is known to increase PR levels in the myometrium.[40-42] Two hours after injection (with either ProGlo or Gd-DO3A), tissues were harvested and imaged with tissues from uninjected mice. The difference in MR contrast between mice injected with ProGlo and those injected with Gd-DO3A is shown in **Figure 5A** and **5B**. The organs from the mouse injected with ProGlo had significantly increased signal intensity compared to tissues from the Gd-DO3A and uninjected mice, particularly in areas that corresponded to the PR-rich myometrium (**Figure 5A**) and the ovarian follicles (**Figure 5B**, blue arrows). Enhancement in signal intensity of the tissues from the Gd-DO3A injected mouse was detected as compared to tissues from the uninjected mouse.

## *ProGlo Preferentially Targets PR(+) Tumors* In Vivo

To determine if ProGlo specifically targets PR(+) tumors compared to PR(-) tumors, ProGlo or Gd-DO3A was injected into nude mice xenografted with PR(+) T47D cells on the right flank and PR(-) MDA-MB-231 cells on the left flank. $T_1$-weighted images of tumor-bearing mice were acquired before injection and 2, 6, and 24 hours after intraperitoneal or subcutaneous injection.

Changes in CNR after injection with Gd-DO3A and ProGlo are shown in **Figure 6A** and **6B**, respectively. Intraperitoneal injection of Gd-DO3A resulted in no significant difference

in average CNR between the two tumors (**Figure 6A**, top graph). Furthermore, the fold change in CNR did not change relative to the preinjection CNR after intraperitoneal injection of Gd-DO3A (**Figure 6A**, bottom graph). ProGlo, by contrast, significantly increased the CNR of the PR(+) tumor relative to the PR(-) tumor 2 and 6 hours after intraperitoneal injection (**Figure 6B**, top graph). In addition, the change in CNR relative to preinjection CNR for the PR(+) tumor was greater than that for the PR(-) tumor (**Figure 6B**, bottom graph). Images of mice injected with Gd-DO3A or ProGlo are represented in **Figure 6C** (top and bottom panels, respectively). These results suggest that ProGlo is significantly more effective than Gd-DO3A at enhancing tumor CNR, particularly in tumors that express high levels of PR.

Mice were injected subcutaneously and imaged with Gd-DO3A (**Figure 7A**) or ProGlo (**Figure 7B**) to study biological effects resulting from a different route of delivery. Subcutaneously injected ProGlo demonstrated targeting to the PR(+) tumor over the PR(-) tumor. The average CNR over four mice (Mouse 4 – Mouse 7) subcutaneously injected with ProGlo increased in the PR(+) tumor after injection, and the average CNR of the PR(+) tumor was significantly higher than the PR(-) tumor 6 hours after ProGlo injection. By 24 hours post-injection, the average CNRs in each tumor were not significantly different and had both returned to preinjection CNR levels. A significant increase in CNR in the PR(-) tumor was not detected after injection of ProGlo. The average CNR over three mice (Mouse 1 – Mouse 3) injected with Gd-DO3A did not significantly change in either tumor. Representative axial images of xenografted mice at each timepoint are shown in **Figure 7C**.

ProGlo overall exhibited increased tumor uptake with specificity for the PR(+) tumor compared to Gd-DO3A regardless of mode of injection. However, subcutaneous injection of ProGlo was associated with less toxicity than intraperitoneal injection (intraperitoneally injected mice did not survive to 24 hours). Autopsies could not define the exact mode of toxicity, but such toxicity was not detected in CD-1 mice regardless of the route of administration or with subcutaneous injections of ProGlo in the nude mice.

## Discussion

Steroid receptors such as PR are significant biomarkers in endometriosis, uterine cancer, and breast cancer that correlate with disease prognosis and therapeutic efficacy.[1, 2] While receptor status is currently determined by immunohistochemistry assays of tissue biopsy samples, there has been interest in developing noninvasive PR imaging agents that would allow for improved molecular characterization, treatment decisions, and repeat analyses.[6] The PR-targeted MR contrast agent ProGlo targeted and enhanced CNR in PR-rich organs *in vivo*. In addition, ProGlo was taken up to a greater extent than the non-targeted Gd-DO3A in tumors, specifically if the tumor expressed PR. To our knowledge, ProGlo is the first steroid-based MRI contrast agent that has successfully targeted and accumulated in PR-rich organs and tumors *in vivo*.

Injection of ProGlo into female mice resulted in accumulation and retention of the agent in several PR-rich tissues, particularly the uterus. High levels of ProGlo in these PR-rich tissues compared to low levels in the muscle (which expresses significantly less PR)[40-42] are evidence of PR-based targeting and retention. In addition, the low levels of ProGlo in other abdominal tissues and fat compared to the uterus indicate that lipophilicity did not significantly contribute the retention of ProGlo in the uterus, ovaries, and mammary tissues. Gd-Hexyl-DO3A and Gd-DO3A, on the other hand, did not reveal any specificity for the PR-rich tissues. Therefore, PR levels play a large role in the distribution of ProGlo without affecting the distribution of the non-targeted agents.

The images of the uteri *in vivo* in CD-1 mice correlated well with the tissue distribution in that they both displayed significant and tissue specific enhancement of Proglo in receptor rich tissues *in vivo*. After injection of ProGlo, the average CNR of the uteri remained higher than the CNR before injection for at least 24 hours. The average CNR did not maintain a higher level after injection of Gd-DO3A over 24 hours. Furthermore, specific accumulation of ProGlo was observed in the PR-rich regions of the uterus and ovarian follicles in *ex vivo* images of the tissues embedded in agarose. These data indicate that ProGlo not only accumulates in PR-rich tissues, but likely distributes itself preferentially in substructures of these tissues with high PR expression. Tissue structure specific imaging would be of interest in MRI-based histology which would use targeted MRI contrast agents to "stain" tissues and create high resolution 3D reconstructions.[43, 44] Unlike traditional histology, these tissues would require no freezing, fixation, or sectioning, which can alter sample morphology and introduce artifacts. Additionally, ProGlo might be employed as a theranostic for detecting, monitoring, and treating uterine-based diseases such as endometriosis and endometrial cancer.

Xenograft images demonstrated targeting of ProGlo to the PR(+) tumor over the PR(-) tumor, while Gd-DO3A did not display preference for either tumor over the other. The differences in CNR between the tumors after subcutaneous injection were lower than after intraperitoneal injection, most likely as a result of the imaging time points. The tissue distribution of the agents after subcutaneous injection specifically in nude mice with estrogen pellets implanted was not determined. Therefore, the optimal imaging times in nude mice after subcutaneous injection, isoflurane exposure, and estrogen supplementation may have differed from the CD-1 mice and nude mice that were injected intraperitoneally. The overall trend revealed that, regardless of delivery route, ProGlo specifically targeted the PR(+) tumor at the 2 and 6 hour time points. More importantly, ProGlo was taken up to a greater extent by the tumors, as shown by the greater change in CNR over the preinjection images than with Gd-DO3A. Therefore, ProGlo not only specifically targets PR(+) tumors, but is an overall improved tumor imaging agent compared to Gd-DO3A likely due to its ability to traverse the cellular membrane.

Intraperitoneal injection of ProGlo in the nude mice was associated with toxicity. The exact cause of death of these mice could not be determined, but may have involved a combination of ProGlo insolubility and the stress of isoflurane. Subcutaneous injection of ProGlo was not associated with toxicity in any of the mice tested, most likely because the agent had limited access to internal organs with this injection method and may have been eliminated by additional mechanisms. Furthermore, intraperitoneal injection of ProGlo was not associated with high toxicity in the CD-1 mice, even those that received isoflurane, indicating that this problem may have been specific to nude mice. Hydrophobic drugs are generally associated with greater toxicity than hydrophilic drugs, and a more water soluble PR-targeted agent would likely alleviate this issue.[36, 37] Water soluble modifications of ProGlo are currently being developed in our group as one method to reduce systemic toxicity.

Finally, while ProGlo and the two non-targeted control agents had similar relaxivities to clinically used Gd(III) agents, the relaxivities for ProGlo and Gd-Hexyl-DO3A were higher than that for Gd-DO3A at 1.41 T. This was due in part to the higher molecular weight of ProGlo and Gd-Hexyl-DO3A. Furthermore, aggregation or micellar formation may have occurred as a result of the amphiphilic nature of these molecules. The increased molecular weight of these complexes in comparison to Gd-DO3A would affect the rotational correlation coefficient ($\tau_R$) of the complex, thus increasing relaxivity.[45, 46] However, while important at lower field strengths, this $\tau_R$ effect is insignificant at the high magnetic field (7 T) used for the *in vivo* images.[47] Further studies are currently being conducted *in vivo* at lower field strength (1.5 or 3 T) to determine whether $\tau_R$ changes further enhance CNR of

PR(+) tissues by increasing the relaxivity of ProGlo, particularly upon binding to PR, which would increase the molecular weight of the complex in comparison to the non-targeted controls.

In conclusion, ProGlo targeted PR-rich tissues *in vivo* and specifically increased CNR in these tissues compared to muscle. Furthermore, ProGlo increased CNR in tumors compared to Gd-DO3A by targeting PR(+) tumors over PR(-) tumors while Gd-DO3A showed preference for neither tumor type. These observations indicate that ProGlo and similar agents could potentially be clinically used to noninvasively diagnose, molecularly characterize, and monitor diseases such as breast, uterine, and ovarian cancers that have altered steroid receptors that directly correlate to disease stage and grade.

## Supplementary Material

Refer to Web version on PubMed Central for supplementary material.

## Acknowledgments

We thank Dr. Teresa Woodruff for helpful advice, Dr. Emily Alex Waters and Dr. Ellen Kohlmeir for helpful discussions and assistance with the acquisition of *in vivo* images, and Taryn Townsend for assistance during the xenografting procedures.

Grant Support

This work was supported by NIH grants R01EB005866, R21CA143331, and by American Cancer Society Illinois Division 08-08. P. A .S. acknowledges support from the CDMRP Breast Cancer Research Program (BC093977) and is an ARCS (Achievement Rewards for College Scientists) Foundation Scholar. A portion of this work was completed at the Northwestern University Integrated Molecular Structure Education and Research Center. A description of the facility and full funding disclosure can be found at http://pyrite.chem.northwestern.edu/analyticalserviceslab/asl.htm. Imaging was performed at the Northwestern University Center for Advanced Molecular Imaging generously supported by NCI CCSG P30 CA060553 awarded to the Robert H Lurie Comprehensive Cancer Center. MRI was performed on the 7T Bruker Pharmascan system purchased with the support of NCRR 1S10RR025624-01. Metal analysis was performed at the Northwestern University Quantitative Bioelemental Imaging Center generously supported by NASA Ames Research Center NNA04CC36G.

## References

1. Ahmad N, Kumar R. Steroid hormone receptors in cancer development: a target for cancer therapeutics. Cancer Lett. 2011; 300(1):1–9. [PubMed: 20926181]
2. Orlando L, Schiavone P, Fedele P, Calvani N, Nacci A, Rizzo P, Marino A, D'Amico M, Sponziello F, Mazzoni E, Cinefra M, Fazio N, Maiello E, Silvestris N, Colucci G, Cinieri S. Molecularly targeted endocrine therapies for breast cancer. Cancer Treat Rev. 2010; 36(Suppl 3):S67–S71. [PubMed: 21129614]
3. Uharcek P. Prognostic factors in endometrial carcinoma. J Obstet Gynaecol Res. 2008; 34(5):776–783. [PubMed: 18958927]
4. Boruban MC, Altundag K, Kilic GS, Blankstein J. From endometrial hyperplasia to endometrial cancer: insight into the biology and possible medical preventive measures. Eur J Cancer Prev. 2008; 17(2):133–138. [PubMed: 18287870]
5. Cui X, Schiff R, Arpino G, Osborne CK, Lee AV. Biology of progesterone receptor loss in breast cancer and its implications for endocrine therapy. J Clin Oncol. 2005; 23(30):7721–7735. [PubMed: 16234531]
6. Lee JH, Zhou HB, Dence CS, Carlson KE, Welch MJ, Katzenellenbogen JA. Development of [F-18]fluorine-substituted Tanaproget as a progesterone receptor imaging agent for positron emission tomography. Bioconjug Chem. 2010; 21(6):1096–1104. [PubMed: 20496889]

7. Osborne CK, Yochmowitz MG, Knight WA 3rd, McGuire WL. The value of estrogen and progesterone receptors in the treatment of breast cancer. Cancer. 1980; 46(12 Suppl):2884–2888. [PubMed: 7448733]
8. Ito K, Utsunomiya H, Yaegashi N, Sasano H. Biological roles of estrogen and progesterone in human endometrial carcinoma--new developments in potential endocrine therapy for endometrial cancer. Endocr J. 2007; 54(5):667–679. [PubMed: 17785917]
9. Hopp TA, Weiss HL, Hilsenbeck SG, Cui Y, Allred DC, Horwitz KB, Fuqua SA. Breast cancer patients with progesterone receptor PR-A-rich tumors have poorer disease-free survival rates. Clin Cancer Res. 2004; 10(8):2751–2760. [PubMed: 15102680]
10. Arpino G, Weiss H, Lee AV, Schiff R, De Placido S, Osborne CK, Elledge RM. Estrogen receptor-positive, progesterone receptor-negative breast cancer: association with growth factor receptor expression and tamoxifen resistance. J Natl Cancer Inst. 2005; 97(17):1254–1261. [PubMed: 16145046]
11. Fuqua SA, Cui Y, Lee AV, Osborne CK, Horwitz KB. Insights into the role of progesterone receptors in breast cancer. J Clin Oncol. 2005; 23(4):931–2. author reply 932-933. [PubMed: 15681552]
12. Osborne CK, Schiff R, Arpino G, Lee AS, Hilsenbeck VG. Endocrine responsiveness: understanding how progesterone receptor can be used to select endocrine therapy. Breast. 2005; 14(6):458–465. [PubMed: 16236516]
13. Montemurro F, Aglietta M. Incorporating trastuzumab into the neoadjuvant treatment of HER2-overexpressing breast cancer. Clin Breast Cancer. 2005; 6(1):77–80. [PubMed: 15899075]
14. Jacobsen BM, Richer JK, Sartorius CA, Horwitz KB. Expression profiling of human breast cancers and gene regulation by progesterone receptors. J Mammary Gland Biol Neoplasia. 2003; 8(3):257–268. [PubMed: 14973372]
15. Hospers GA, Helmond FA, de Vries EG, Dierckx RA, de Vries EF. PET imaging of steroid receptor expression in breast and prostate cancer. Curr Pharm Des. 2008; 14(28):3020–3032. [PubMed: 18991716]
16. Mankoff DA, Link JM, Linden HM, Sundararajan L, Krohn KA. Tumor receptor imaging. J Nucl Med. 2008; 49(Suppl 2):149S–163S. [PubMed: 18523071]
17. Zhou D, Carlson KE, Katzenellenbogen JA, Welch MJ. Bromine- and iodine-substituted 16alpha, 17alpha-dioxolane progestins for breast tumor imaging and radiotherapy: synthesis and receptor binding affinity. J Med Chem. 2006; 49(15):4737–4744. [PubMed: 16854080]
18. Dehdashti F, McGuire AH, Van Brocklin HF, Siegel BA, Andriole DP, Griffeth LK, Pomper MG, Katzenellenbogen JA, Welch MJ. Assessment of 21-[18F]fluoro-16 alpha-ethyl-19-norprogesterone as a positron-emitting radiopharmaceutical for the detection of progestin receptors in human breast carcinomas. J Nucl Med. 1991; 32(8):1532–1537. [PubMed: 1869974]
19. Verhagen A, Studeny M, Luurtsema G, Visser GM, De Goeij CC, Sluyser M, Nieweg OE, Van der Ploeg E, Go KG, Vaalburg W. Metabolism of a [18F]fluorine labeled progestin (21-[18F]fluoro-16 alpha-ethyl-19-norprogesterone) in humans: a clue for future investigations. Nucl Med Biol. 1994; 21(7):941–952. [PubMed: 9234348]
20. Margolis DJ, Hoffman JM, Herfkens RJ, Jeffrey RB, Quon A, Gambhir SS. Molecular imaging techniques in body imaging. Radiology. 2007; 245(2):333–356. [PubMed: 17940297]
21. Steinert HC. PET and PET-CT of Lung Cancer. Methods Mol Biol. 2011; 727:33–51. [PubMed: 21331927]
22. Tan EH, Goh SW. Exploring new frontiers in molecular imaging: Emergence of Ga PET/CT. World J Radiol. 2010; 2(2):55–67. [PubMed: 21160919]
23. Wehrl HF, Judenhofer MS, Wiehr S, Pichler BJ. Pre-clinical PET/MR: technological advances and new perspectives in biomedical research. Eur J Nucl Med Mol Imaging. 2009; 36(Suppl 1):S56–68. [PubMed: 19194703]
24. Lewis JS, Achilefu S, Garbow JR, Laforest R, Welch MJ. Small animal imaging. current technology and perspectives for oncological imaging. Eur J Cancer. 2002; 38(16):2173–2188. [PubMed: 12387842]
25. de Kemp RA, Epstein FH, Catana C, Tsui BM, Ritman EL. Small-animal molecular imaging methods. J Nucl Med. 2010; 51(Suppl 1):18S–32S. [PubMed: 20457793]

26. Major JL, Meade TJ. Bioresponsive, cell-penetrating, and multimeric MR contrast agents. Acc Chem Res. 2009; 42(7):893–903. [PubMed: 19537782]
27. Frullano L, Meade TJ. Multimodal MRI contrast agents. J Biol Inorg Chem. 2007; 12(7):939–949. [PubMed: 17659368]
28. Lehman CD, Gatsonis C, Kuhl CK, Hendrick RE, Pisano ED, Hanna L, Peacock S, Smazal SF, Maki DD, Julian TB, DePeri ER, Bluemke DA, Schnall MD. MRI evaluation of the contralateral breast in women with recently diagnosed breast cancer. N Engl J Med. 2007; 356(13):1295–1303. [PubMed: 17392300]
29. Tozaki M. Diagnosis of breast cancer: MDCT versus MRI. Breast Cancer. 2008; 15(3):205–211. [PubMed: 18443898]
30. Cooper KL, Meng Y, Harnan S, Ward SE, Fitzgerald P, Papaioannou D, Wyld L, Ingram C, Wilkinson ID, Lorenz E. Positron emission tomography (PET) and magnetic resonance imaging (MRI) for the assessment of axillary lymph node metastases in early breast cancer: systematic review and economic evaluation. Health Technol Assess. 2011; 15(4):iii–iv. 1–134.
31. Lee JM, Kopans DB, McMahon PM, Halpern EF, Ryan PD, Weinstein MC, Gazelle GS. Breast cancer screening in BRCA1 mutation carriers: effectiveness of MR imaging--Markov Monte Carlo decision analysis. Radiology. 2008; 246(3):763–771. [PubMed: 18309013]
32. Lee J, Zylka MJ, Anderson DJ, Burdette JE, Woodruff TK, Meade TJ. A steroid-conjugated contrast agent for magnetic resonance imaging of cell signaling. J Am Chem Soc. 2005; 127(38): 13164–13166. [PubMed: 16173742]
33. Lee J, Burdette JE, MacRenaris KW, Mustafi D, Woodruff TK, Meade TJ. Rational design, synthesis, and biological evaluation of progesterone-modified MRI contrast agents. Chem Biol. 2007; 14(7):824–834. [PubMed: 17656319]
34. Saha P, Hodl C, Strauss WSL, Steiner R, Goessler W, Kunert O, Leitner A, Haslinger E, Schramm HW. Synthesis, in vitro progesterone receptors affinity of gadolinium containing mifepristone conjugates and estimation of binding sites in human breast cancer cells. Bioorgan Med Chem. 2010; 18(5):1891–1898.
35. Couture JF, Legrand P, Cantin L, Luu-The V, Labrie F, Breton R. Human 20alpha-hydroxysteroid dehydrogenase: crystallographic and site-directed mutagenesis studies lead to the identification of an alternative binding site for C21-steroids. J Mol Biol. 2003; 331(3):593–604. [PubMed: 12899831]
36. Leo A, Hansch C, Elkins D. Partition Coefficients and Their Uses. Chem Rev. 1971; 71(6):525–616.
37. Leeson PD, Springthorpe B. The influence of drug-like concepts on decision-making in medicinal chemistry. Nat Rev Drug Discov. 2007; 6(11):881–890. [PubMed: 17971784]
38. Nunez FAA, Yalkowsky SH. Correlation between log P and ClogP for some steroids. J Pharm Sci. 1997; 86(10):1187–1189. [PubMed: 9344178]
39. van De Waterbeemd H, Smith DA, Beaumont K, Walker DK. Property-based design: optimization of drug absorption and pharmacokinetics. J Med Chem. 2001; 44(9):1313–1333. [PubMed: 11311053]
40. Uotinen N, Puustinen R, Pasanen S, Manninen T, Kivineva M, Syvala H, Tuohimaa P, Ylikomi T. Distribution of progesterone receptor in female mouse tissues. Gen Comp Endocrinol. 1999; 115(3):429–441. [PubMed: 10480995]
41. Tibbetts TA, Mendoza-Meneses M, O'Malley BW, Conneely OM. Mutual and intercompartmental regulation of estrogen receptor and progesterone receptor expression in the mouse uterus. Biol Reprod. 1998; 59(5):1143–1152. [PubMed: 9780321]
42. Mulac-Jericevic B, Mullinax RA, DeMayo FJ, Lydon JP, Conneely OM. Subgroup of reproductive functions of progesterone mediated by progesterone receptor-B isoform. Science. 2000; 289(5485):1751–1754. [PubMed: 10976068]
43. Johnson GA, Cofer GP, Fubara B, Gewalt SL, Hedlund LW, Maronpot RR. Magnetic resonance histology for morphologic phenotyping. J Magn Reson Imaging. 2002; 16(4):423–429. [PubMed: 12353257]

44. Johnson GA, Ali-Sharief A, Badea A, Brandenburg J, Cofer G, Fubara B, Gewalt S, Hedlund LW, Upchurch L. High-throughput morphologic phenotyping of the mouse brain with magnetic resonance histology. Neuroimage. 2007; 37(1):82–89. [PubMed: 17574443]

45. Caravan P, Ellison JJ, McMurry TJ, Lauffer RB. Gadolinium(III) Chelates as MRI Contrast Agents: Structure, Dynamics, and Applications. Chem Rev. 1999; 99(9):2293–2352. [PubMed: 11749483]

46. Meade TJ, Taylor AK, Bull SR. New magnetic resonance contrast agents as biochemical reporters. Curr Opin Neurobiol. 2003; 13(5):597–602. [PubMed: 14630224]

47. Caravan P, Farrar CT, Frullano L, Uppal R. Influence of molecular parameters and increasing magnetic field strength on relaxivity of gadolinium- and manganese-based T1 contrast agents. Contrast Media Mol Imaging. 2009; 4(2):89–100. [PubMed: 19177472]

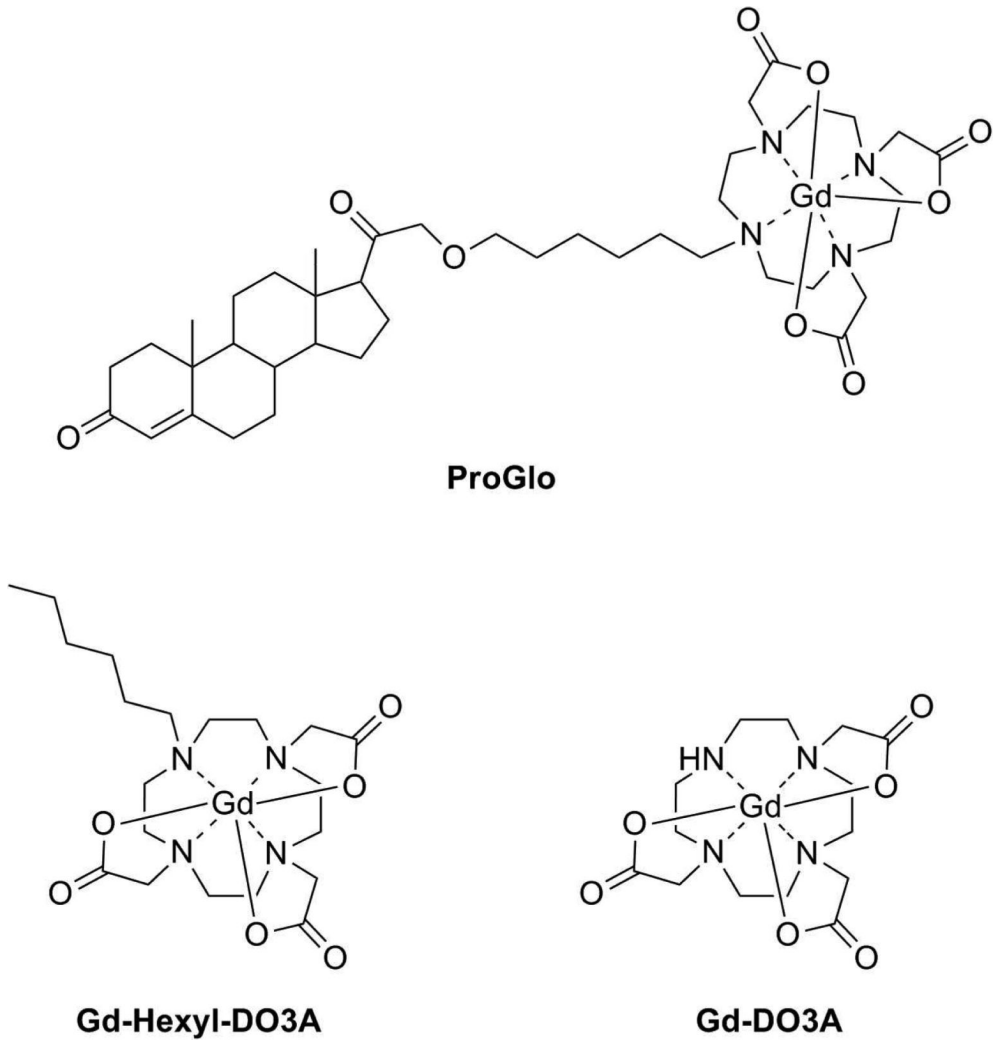


**Figure 1.**
Structures of the progesterone-modified and non-targeted MR contrast agents used in this study.

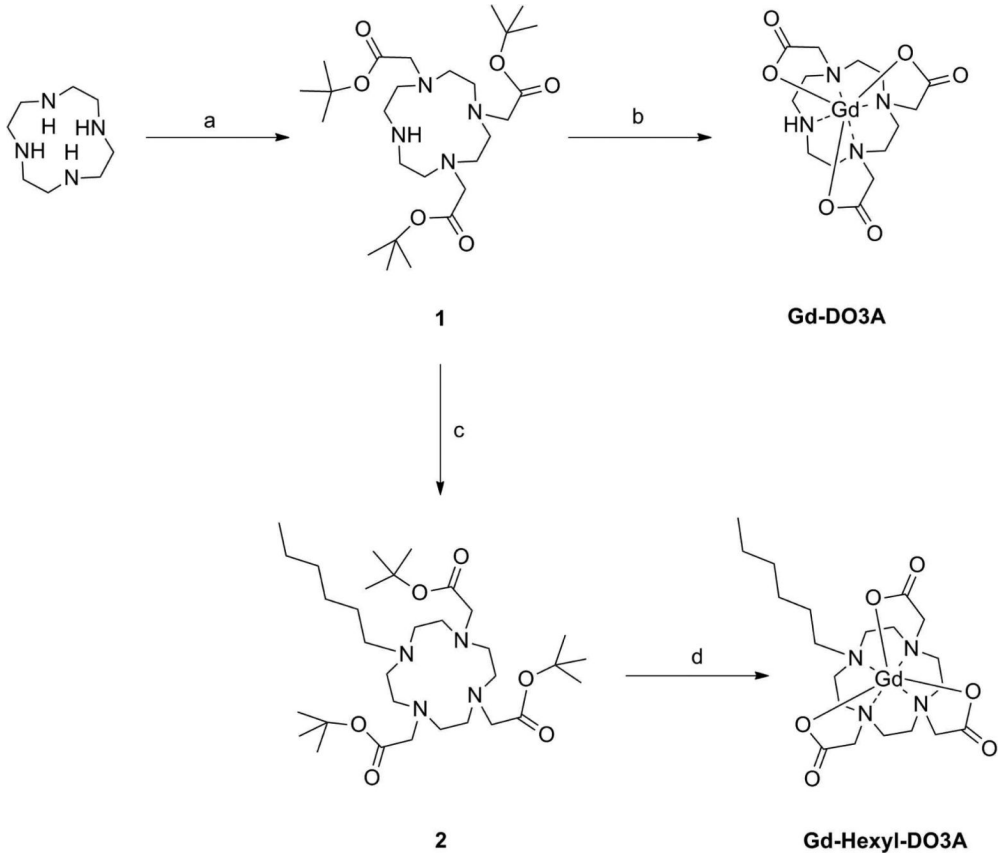


**Scheme 1.**

Synthesis of the non-targeted control agents Gd-DO3A and Gd-Hexyl-DO3A. Reagents and Conditions: (a) tert-butylbromoacetate, $NaHCO_3$, 40%; (b) 1. Trifluoroacetic acid, 2. $GdCl_3$, $H_2O$, pH = 5.5 – 6.5, 60 °C, 94 % over two steps; (c) 1-bromohexane, $K_2CO_3$, $NBu_4OH$, 65 °C, 55%; (d) 1. Formic acid, 60 °C, 2. $GdCl_3$, $H_2O$, pH = 5.5 – 6.5, 60 °C, 44% over two steps.

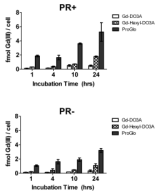


**Figure 2.**

Time-dependent cellular uptake of Gd-DO3A, Gd-Hexyl-DO3A, and ProGlo in PR(+) T47D human breast cancer cells (top) and PR(-) MDA-MB-231 human breast cancer cells (bottom). Cellular uptake of ProGlo was significantly higher than Gd-Hexyl-DO3A and Gd-DO3A in both cell lines (Student's t test, $p < 0.05$). Data are mean ± standard deviation.

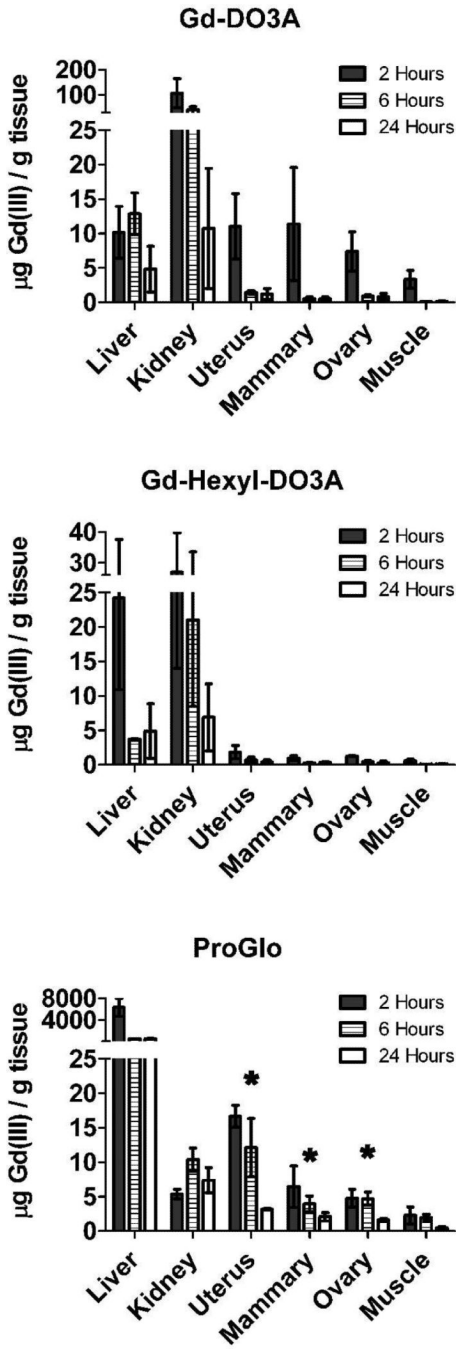


**Figure 3.**

Tissue distribution of Gd-DO3A (top), Gd-Hexyl-DO3A (middle), and ProGlo (bottom) in female CD-1 mice 2, 6, and 24 hours after injection. The levels of Gd(III) in the PR-rich tissues (uterus, ovaries, and mammary tissues) were significantly higher than in the muscle (which served as a negative control due to its low PR expression) at all time points after injection of ProGlo (Student's t test, $p < 0.05$). The levels of Gd(III) in the PR-rich tissues after injection of ProGlo were significantly higher than the levels after injection of Gd-DO3A after 2 hours (Student's t test, $p < 0.05$). Asterisks designate high retention of ProGlo in PR-rich tissues. Data are mean ± standard deviation.

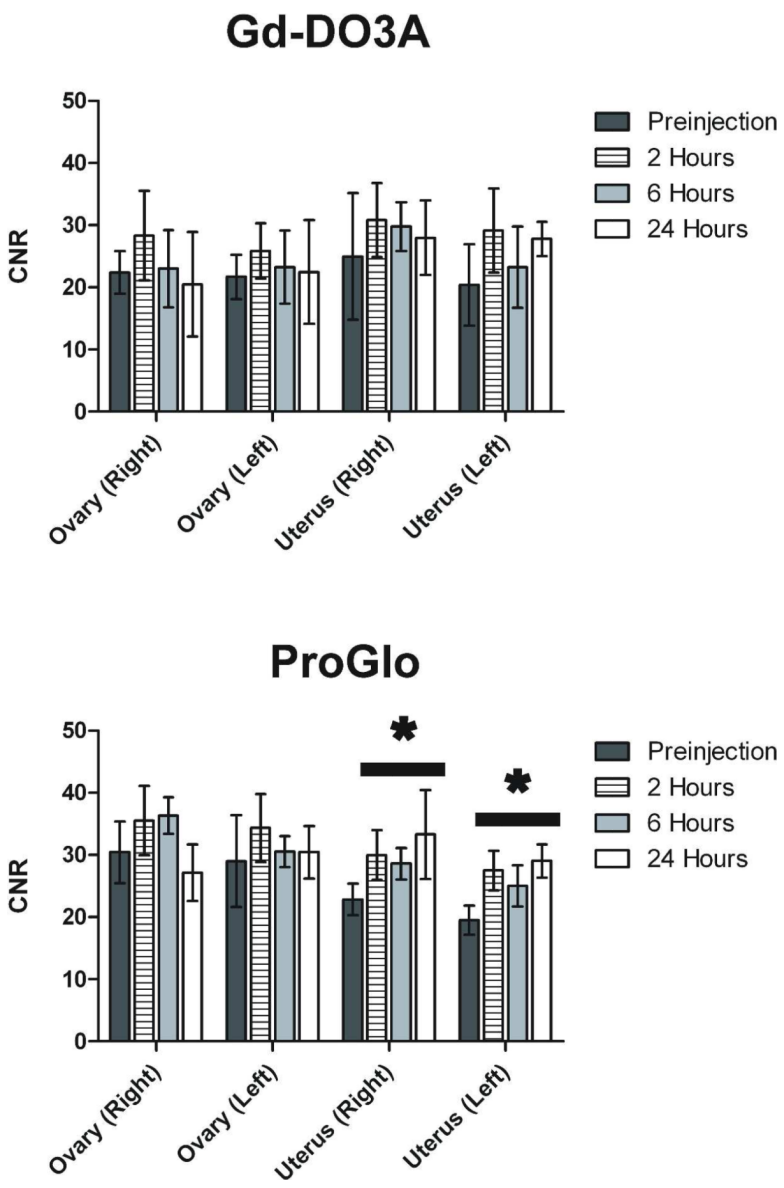


**Figure 4.**

Enhancement in contrast-to-noise ratios (CNRs) in the uterus and ovaries after injection of Gd-DO3A or ProGlo in female CD-1 mice. A, Average CNR of ovaries and uteri in vivo after injection of Gd-DO3A (left) or ProGlo (right). A significant increase in the CNR of the uteri was observed after injection of ProGlo (black bars with asterisks, Student's t test, $p < 0.05$) and was maintained for at least 24 hour post-injection. Data are mean ± standard deviation.

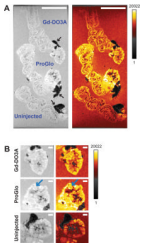


**Figure 5.**

*Ex vivo* images of the uterus and ovaries after injection of Gd-DO3A or ProGlo in superovulated female CD-1 mice. A, *Ex vivo* images of the uterus and ovaries harvested 2 hours after injection with Gd-DO3A (top), injection with ProGlo (middle), or no injection (bottom). Black arrows designate fat. Color images highlight areas of increased signal intensity (calibration bar represents signal intensity in arbitrary units). White scale bars represent 5 mm. B, *Ex vivo* images of the ovaries after injection with Gd-DO3A (top), injection with ProGlo (middle), or no injection (bottom). Blue arrows highlight ovarian follicles. White scale bars represent 1 mm.

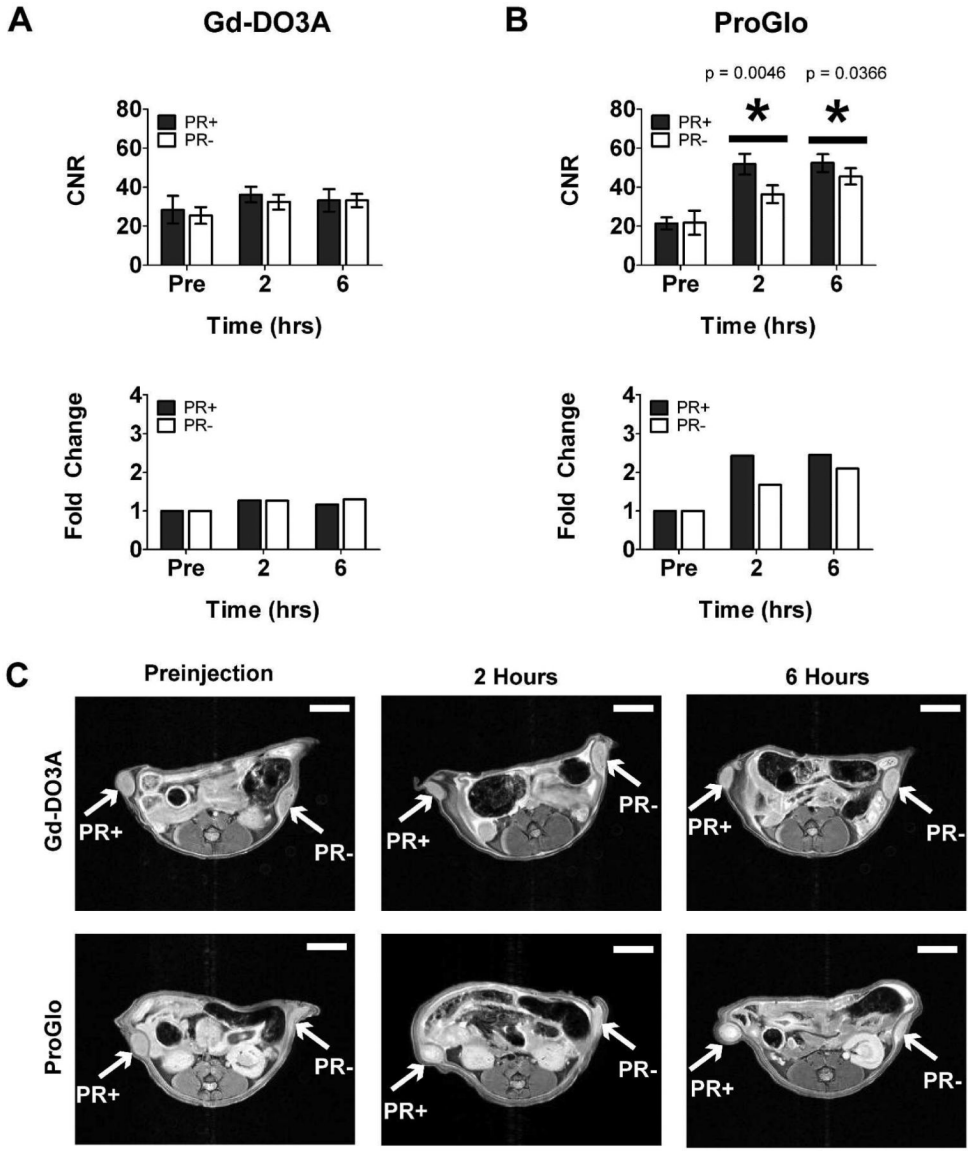


**Figure 6.**

Contrast-to-noise ratios (CNRs) in tumor xenografts after intraperitoneal injection of Gd-DO3A or ProGlo in female nude mice. A, Average CNR of PR(+) or PR(-) tumors over time after intraperitoneal injection of Gd-DO3A (top) and change in average CNR compared to the average preinjection CNR (bottom). B, Average CNR of PR(+) or PR(-) tumors over time after intraperitoneal injection of ProGlo (top) and the fold change in CNR over the preinjection (pre) levels (bottom). Significant CNR enhancement was seen after intraperitoneal injection of ProGlo in the PR(+) tumor over the PR(-) tumor at 2 and 6 hours post-injection (asterisks, top graph, Student's t test, $p < 0.05$). Data are mean ± standard deviation. P-values (Student's t test, $p < 0.05$) are shown in the graph. C, Representative images of xenografted mice injected intraperitoneally with Gd-DO3A (top panels) or ProGlo (bottom panels). White scale bars represent 5 mm.

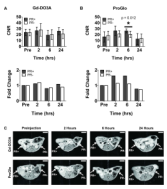

**Figure 7.**

Average contrast-to-noise ratios (CNRs) and fold change in CNRs in tumor xenografts after subcutaneous injection of Gd-DO3A or ProGlo. A, Subcutaneous injection of Gd-DO3A demonstrated no significant enhancement in CNR of PR(+) or PR(-) tumors over time. B, Subcutaneous injection of ProGlo showed specific CNR enhancement in the PR(+) tumor over the PR(-) tumor at 6 hours post-injection (asterisk, Student's t-test, $p < 0.05$). Error bars represent ± standard deviation of the mean. C, Representative images of xenografted mice injected subcutaneously with Gd-DO3A (top panels) or ProGlo (bottom panels). White scale bars represent 5 mm.

**Table 1**

Relaxivities and Octanol-Water Partition Coefficients

| | $r_1$ ($mM^{-1}s^{-1}$) | $r_2$ ($mM^{-1}s^{-1}$) | LogP |
|---|---|---|---|
| **ProGlo** | 4.73[a], 5.35 ± 0.74[b] | 6.14 ± 0.81[b] | 1.40 ± 0.08 |
| **Gd-Hexyl-DO3A** | 5.55 ± 0.22[c] | 6.38 ± 0.38[c] | -1.21 ± 0.12 |
| **Gd-DO3A** | 4.05 ± 0.02[c] | 4.75 ± 0.35[c] | -2.96 ± 0.35 |
| **21-Hydroxyprogesterone** | --- | --- | 2.88[d] |

[a] Measured at 4.7 T (200 MHz), 21 °C[33]

[b] Measured in 1% DMSO in water, 1.41 T (60 MHz), 37 °C

[c] Measured in water, 1.41 T (60 MHz), 37 °C

[d] Measured by shake flask method/mass[38]